IN VIVO IMAGING METHODS FOR STUDYING HOST-MICROBIOTA INTERACTIONS

PhD thesis

Dr. Dávid Szöllősi

Doctoral School of Theoretical and Translational Medicine

Semmelweis University

Supervisor: Krisztián Szigeti PhD

Official reviewers: Attila Bóta PhD, DSc
Éva Pállinger PhD

Head of the Complex Examination Committee:
Gábor Varga PhD, DSc

Members of the Complex Examination Committee:
Csaba Ambrus PhD
Barna Vásárhelyi PhD, DSc

Budapest
2024

1. Introduction

Sepsis associated encephalopathy (SAE) is a neuroinflammatory disease caused by sepsis. There is an ongoing effort to develop methods to detect neuroinflammation using molecular imaging. The tracer [^{123}I]CLINME produced promising results in the rat model of unilateral excitotoxic brain lesion, but has not been evaluated in SAE.

Bacterial outer membrane vesicles (OMVs) are emerging as a promising vaccine and drug delivery platform while also having perspective as disease biomarkers and therapeutic targets. Our knowledge regarding their biodistribution is limited and the most widely used methods to measure it have big limitations. Nuclear medicine imaging may offer a solution. A relatively new and exciting approach in extracellular vesicle imaging is the use of genetic engineering to modify the source organism so that it produces a protein which facilitates the radiolabeling. The combination of an autotransporter-based surface display system (such as ones based on AIDA-I or Hbp) combined with a protein ligation system (e.g. SpyCatcher/SpyTag) can be used to anchor large proteins or non-peptide molecules on the bacterial (and OMV) surface. Using these methods it would be possible to decorate the OMV surface with a chelator, enabling highly specific and efficient radiolabeling.

Escherichia coli BL21(DE3) is a fast-growing strain with particularly useful phenotypic traits for protein expression. Its reduced OMV yield can be counteracted using genetic engineering, for example the deletion of the *nlpI* gene. A challenge in OMV based pharmaceutical development is the immunogenicity of OMVs resulting from their high LPS content. There exist genetic engineering solutions to ameliorate the endotoxic effects of *E. coli* LPS. One possibility is the deletion of the *lpxM* gene, blocking the

myristoylation of LPS, leading to a phenotype with lower endotoxicity in humans.

2. Objectives

Our detailed goals are the following:

1. Develop an efficient radiolabeling method for in vivo imaging of OMVs, as summarized in Fig. 1:
    - Use genetic engineering to delete the nlpI and LpxM genes from E. coli BL21(DE3) to create a strain suitable for high yield OMV production and heterologous protein expression while having reduced immunogenicity.
    - Anchor SpyCatcher to the OMV surface using an autotransporter-based surface display system.
    - Create SpyTag-NODAGA-based bifunctional chelators that bind to the SpyCatcher-displaying OMVs, facilitating radiolabeling.
    - Label the OMVs with ^{64}Cu and characterize the radiolabeling.
    - Use PET/MRI to measure the biodistribution of labeled OMVs.
2. Test if [^{125}I]CLINME SPECT can be used to detect early neuroinflammatory changes in a murine model of SAE.

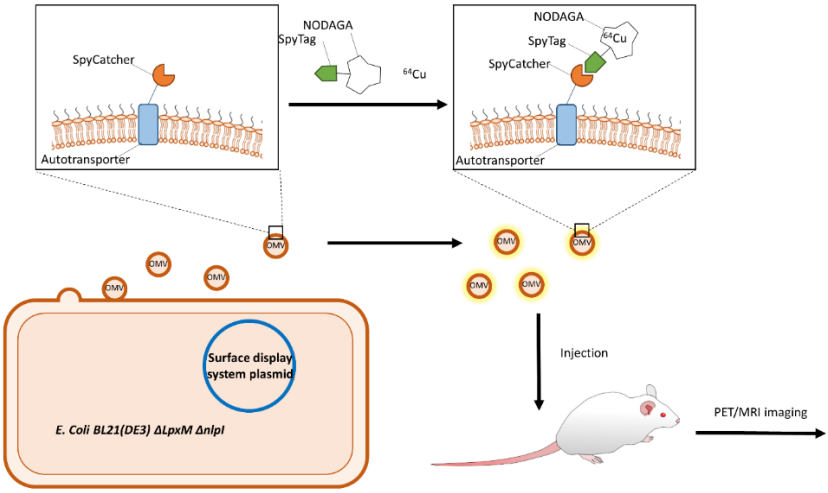

Fig. 1. ***Illustration of the proposed OMV radiolabeling method***. *E. coli BL21(DE3) ΔnlpI, ΔLpxM cells harboring a surface display plasmid express an autotransporter-SpyCatcher fusion protein that integrates into the outer membrane. A synthetic SpyTag-NODAGA bifunctional chelator labeled with 64Cu can covalently bind to the OMV surface with high specificity. The precise biodistribution of these radiolabeled OMVs can be measured using PET/MRI multimodal imaging.*

3. Methods

3.1. Imaging of bacterial OMVs

3.1.1. Culture conditions

For all bacterial liquid cultures lysogeny broth (LB) was used as a medium. Ampicillin, kanamycin or chloramphenicol were used at concentrations of 100 µg/ml, 50 µg/ml, and 34 µg/ml respectively when necessary. Induction of bacteria harboring SpyCatcher surface display plasmids with isopropyl β-d-1-thiogalactopyranoside (IPTG, Thermo Scientific) was carried out at $OD_{600} \approx 0.7$ when required. Bacteria were

cultured for 16 h (following induction) at 37°C with shaking at 180 RPM if otherwise not specified.

3.1.2. Preparation of BL21(DE3) *ΔnlpI, ΔLpxM*

Lambda Red genome editing was used to create two knockout mutations in *E. coli* BL21(DE3) cells following the method described by Sheila Jensen and Alex Nielsen, using the thermosensitive helper plasmid pSIJ8. The genes *nlpI* and *lpxM* were sequentially deleted using PCR-products from Keio collection strains containing kanamycin resistance cassettes at the *nlpI* or *lpxM* locus respectively. The resulting double mutant BL21(DE3) *ΔnlpI, ΔlpxM* was verified using PCR and sequencing. The novel strains was designated BL21.V.

3.1.3. OMV isolation

Cultures were centrifuged and filtered to remove bacteria. Next, the sterile supernatant was concentrated using stirred-cell ultrafiltration followed by tangential flow filtration and ultracentrifugation. For small samples only the ultracentrifugation step was used. The pellet was resuspended in phosphate buffered saline (PBS) and then filtered. In the final step the samples were purified using size exclusion chromatography (SEC).

3.1.4. Analytical methods

Sodium dodecyl sulfate-polyacrylamide gel electrophoresis (SDS-PAGE) was used as a general post-isolation quality control step and to analyze OMV surface display of SpyCatcher. For OMVs, 10% resolving and 5% stacking polyacrylamide gels were used.

OMV size distribution was determined using transmission electron microscopy (TEM) with negative staining.

Size exclusion HPLC (SEC-HPLC) with Sepharose CL-4B (Cytiva, Germany) was generally used for the quality control of OMV isolates and to

analyze SpyCatcher-displaying OMVs following fluorescent or radioactive labeling. Reversed-phase HPLC (RP-HPLC) a Chromolith FastGradient RP-18e 50-2 mm column (Supelco, USA) and a gradient elution protocol was used to check the quality of synthetic peptides and the results of peptide radiolabeling.

3.1.5. Synthesis of labeled SpyTag variants

We synthetized both fluorescent (SpT-CF) and chelator-conjugated SpyTag variants (SpT-3-NODAGA nad SpT-23-NODAGA) to analyze OMV SpyCatcher display and to carry out the radiolabeling procedure.

3.1.6. Construction of surface display plasmids

To anchor SpyCatcher to the OM, we created two different SpyCatcher-autotransporter fusion proteins based on AIDA-I and Hbp using restriction cloning. The *SpyCatcher* gene was inserted into pAIDA1 and into pHbpD(Δd1) to create the plasmids pAIDA-SpC and pHbpD-SpC respectively. The resulting fusion genes (*AIDA-SpyCatcher and HbpD-SpyCatcher*) were then inserted into the pET28a vector to create the plasmids pET28-ASpC and pET28-HSpC respectively. Transcription from these plasmids in *E. coli* BL21.V are inducible using IPTG.

3.1.7. Evaluating SpT-NODAGA binding on OMVs

A simplified binding assay was used to compare the affinity of SpT-3-NODAGA and SpT-23-NODAGA. Samples of SpyCatcher-displaying OMVs were incubated with each SpT-NODAGA variant for 24 hours followed by SpT-CF labeling and SDS-PAGE.

3.1.8. Radiolabeling OMVs

Two different methods were evaluated for OMV radiolabeling. In *Method 1* SpyCatcher-displaying OMVs were first incubated with each SpT-

NODAGA variant followed by the removal of excess peptide using a Sepharose CL-4B column and labeling with 142.5 ± 0.7 MBq $^{64}CuCl_2$. Radiochemical purity (RCP) was measured with SEC-HPLC. Free ^{64}Cu was removed using a Sepharose CL-4B column and serum stability was measured by mixing 20 µl of the labeled OMV sample with 80 µl fetal bovine serum and incubated at 37 °C 300 RPM shaking.

In *Method 2,* SpT-3-NODAGA and SpT-23-NODAGA were first labeled with $^{64}CuCl$ and then mixed with SpyCatcher-expressing OMVs. Radiochemical purity was measured at 1, 2, and 4 hours post-incubation. For negative control, OMVs from the same isolates were pre-incubated with 10 µM SpT-CF for 24 h at 4 °C on an orbital shaker to block available SpyCatcher binding sites.

3.1.9. In vivo imaging of OMVs

Four healthy 21-week-old male BALB/c mice were used for the biodistribution studies. A volume of 120 µl radiolabeled sample (radiolabeled SpT-3/23-NODAGA or OMVs) with an activity of 10.17 ± 1.10 MBq was administered intravenously into the lateral tail vein. Mice were anesthetized with isoflurane for the whole duration of imaging. PET/MRI acquisitions were carried out using a nanoScan PET/MRI 3T (Mediso, Hungary).

3.2. Systemic inflammation

3.2.1. SAE model

Six adult female C57BL/6 mice (n=3 control, n=3 LPS-treated) were used to evaluate [^{125}I]CLINME for the detection of early neuroinflammatory signs in SAE. The SAE model was induced by 3.3 mg/kg body weight of LPS via tail vein injection.

3.2.2. [^{125}I]CLINME preparation and imaging

CLINME molecules were radiolabeled using 195.7 MBq [^{125}I]NaI by the classic chloramine-T method. The radiochemical purity was 95%.

Mice were anesthetized with isoflurane. Before imaging 9.53±0.55 MBq [^{125}I]CLINME was administered intravenously following the subcutaneous injection of 14 mg/kg body weight of potassium perchlorate. SPECT/CT acquisition started 5 h following LPS injection using a NanoSPECT/CT (Silver Upgrade, Mediso Ltd., Budapest). MRI measurements were performed on nanoScan® PET/MRI (Mediso Ltd., Hungary). Brain segmentation into 3D volumes of interest (cerebrum – indicates the whole brain without cerebellum –, cerebellum, cerebral cortex and hippocampus) was performed using a connected threshold algorithm based on MRI image volumes after coregistration with SPECT/CT images in VivoQuant software (inviCRO, US).

4. Results

4.1. Imaging of bacterial OMVs

4.1.1. Characterization of *E. coli* BL21.V OMVs

OMV size distribution was determined using crude OMV samples without purification to avoid a possible bias that could be introduced by filtration (Fig. 2). The results reveal an average OMV diameter of 22.22 ± 9.02 nm which is on the smaller side of previously reported OMV size ranges that typically fall within 10 nm to 300 nm.

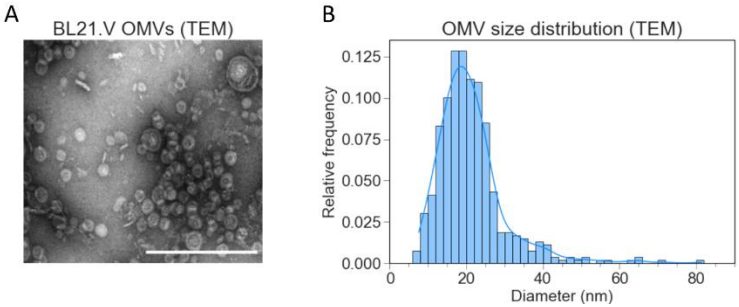

Fig 2. ***OMV characterization results***. ***A)*** *TEM photomicrograph of a crude OMV suspension. The scale bar represents 200 nm.* ***B)*** *Size distribution of OMVs measured on TEM images. Bars represent the histogram; the solid blue line is the result of kernel density estimation.*

4.1.2. Optimization of SpyCatcher surface display

To anchor SpyCather to the OMV surface, it was genetically fused to two different autotransporters. Four different plasmids were compared including two with their originally published backbones (pAIDA-SpC and pHbpD-SpC), and two with pET based backbones (pET28-ASpC and pET28-HSpC) to find the best one. Based on their effect on OMV yield and OMV surface display efficiency we chose pET28-ASpC for our radiolabeling experiments.

4.1.3. Radiolabeling of OMVs

We designed two different chelator-conjugated SpyTag variants, SpT-3-NODAGA and SpT-23-NODAGA. Using a simplified binding assay, both SpT-3-NODAGA and SpT-23-NODAGA showed binding to SpyCatcher-displaying OMVs, with SpT-3-NODAGA demonstrating significantly better results.

We evaluated both variants for radiolabeling. The first radiolabeling approach (*Method 1*) initially resulted in 32.90% RCP and 43.17% RCP for SpT-3-NODAGA and SpT-23-NODAGA labeled OMVs respectively, and 100% RCP after purification. The overall radiolabeling efficiency was 29.20% and 28.87% for SpT-3-NODAGA and SpT-23-NODAGA respectively. Statistical analysis revealed a significant decrease in serum stability from 3 to 24 hours post-incubation amounting to a 0.51% decrease in RCP per hour (95% confidence interval: [0.43%, 0.58%]). Labeling with SpT-3-NODAGA also resulted in a significantly lower overall RCP compared to SpT-23-NODAGA during this time (71.86 ± 4.45% and 79.36 ± 3.96% respectively, $p = 0.0002$). In the second approach (*Method 2*) ^{64}Cu-labeled peptides were incubated with the OMVs, and although both peptides showed significant RCP increase in time, unfortunately even after 4h incubation RCP was still much lower than using *Method 1* (15.26% ± 0.21% for [^{64}Cu]SpT-3-NODAGA and 11.12% ± 0.12% for [^{64}Cu]SpT-23-NODAGA).

4.1.4. In vivo imaging of OMV distribution

The biodistribution of radiolabeled OMVs (*Method 1*) in mice was measured using PET/MRI in three different time points (3h, 6h, 12h post injection). The results are summarized in Fig. 3. In all time points, the uptake of liver and spleen was the highest for radiolabeled OMVs regardless of the SpT-NODAGA variant used. The biodistribution of radiolabeled peptides without OMVs was also investigated and showed a very different pattern with the highest organ uptake measured in the kidneys, decreasing with time. This suggests that the peptides are eliminated mainly through renal clearance.

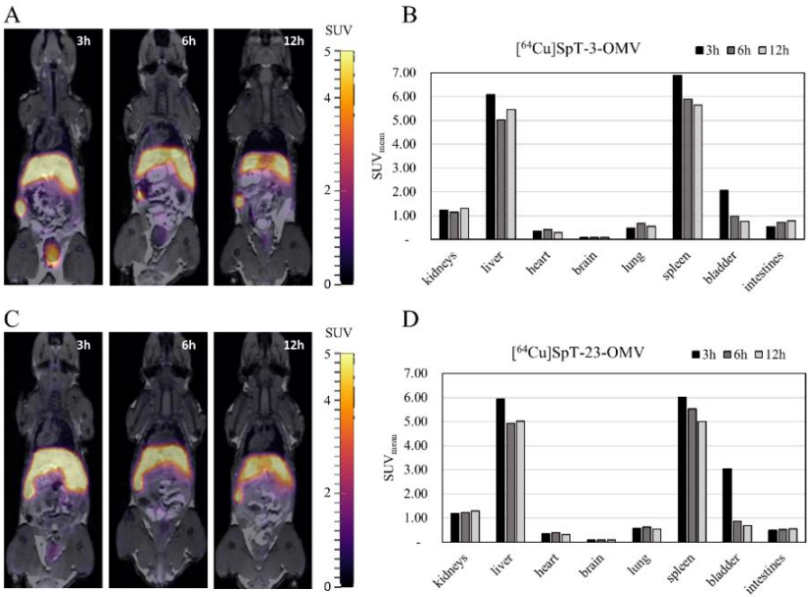

Fig. 3. ***In vivo biodistribution of radiolabeled OMVs in mice. A and C)*** *PET/MRI at 3, 6, and 12 hours p.i. of SpT-3-NODAGA and SpT-23-NODAGA OMVs, respectively.* ***B and D)*** *Decay-corrected organ uptakes (SUV_{mean}) of SpT-3-NODAGA and SpT-23-NODAGA OMVs, respectively .*

4.2 . Systemic inflammation

[^{125}I]CLINME SPECT results obtained from SAE mice are shown in Fig. 4. Significantly elevated (p = 0.05) uptake was observed in the cerebrum (4.23 × 10-3 ± 0.17 × 10-3 ml-1 and 5.10 × 10-3 ± 0.49 × 10-3 ml-1 for control and LPS treated respectively) and non-significant elevation in all other investigated brain areas.

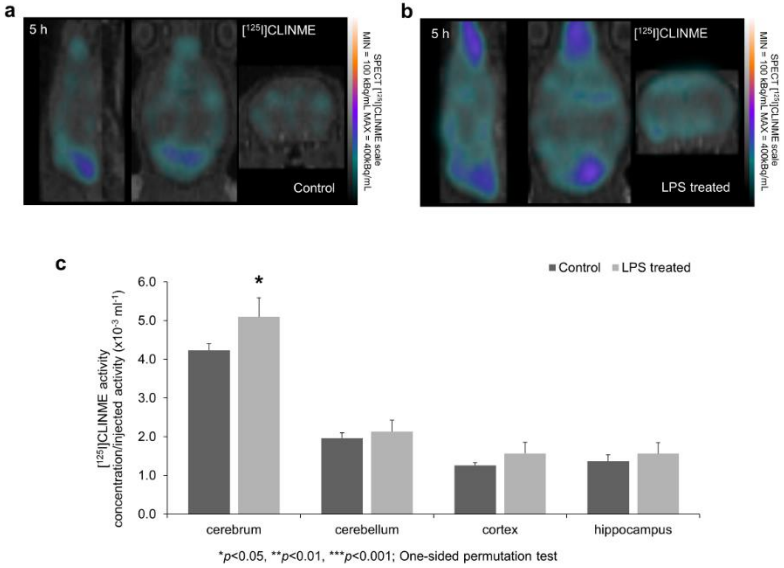

Fig. 4. ***Brain [^{125}I]CLINME uptake in mice measured with SPECT.*** *SPECT coregistration with MRI showing [^{125}I]CLINME uptake changes after* ***A)*** *LPS-induced neuroinflammation compared to* ***B)*** *the control group. Arrows indicate example areas where the difference in radiotracer uptakes between the two groups is visually discernable.* ***C)*** *[^{125}I]CLINME uptake is significantly increased 5h after the LPS injection in the cerebrum (*p≤0.05 – One-sided permutation test).*

5. Conclusions

In conclusion, our results provide new possibilities for the *in vivo* imaging of different aspects of host-microbiota interactions.

First of all, we have shown that the combination of a surface display system with a protein ligation system and a chelator enables specific and stable OMV radiolabeling suitable for molecular imaging. The modularity of our approach results in great versatility as these three main parts can be customized. Our method could also be used as an "imaging module" for OMV based drug carrier and vaccine development, where bioengineered OMVs are often decorated with a protein ligation system into which the SpyCatcher-SpyTag-NODAGA system can be incorporated.

Secondly, we have shown that radioiodinated CLINME can detect the early increase in cerebral TSPO binding sites associated with the neuroinflammatory changes present during sepsis. This proves the usefulness of a versatile radiotracer which can be used for both SPECT and PET imaging depending on the choice of iodine isotope.

Achievements:

1) A novel bacterial strain, *E. coli* BL21.V was designed.
2) The OMVs of *E. coli* BL21.V have been characterized.
3) The SpyCatcher-SpyTag protein ligation system combined with an autotransporter-based surface display system can be used for OMV radiolabeling.
4) [^{125}I]CLINME SPECT can be used to detect the early neuroinflammatory effects of systemic inflammation in mice.

6. Bibliography of the candidate's publications

Publications related to the thesis

1. Szöllősi, D., P. Hajdrik, H. Tordai, I. Horváth, D. Veres, B. Gillich, K.D. Shailaja, L. Smeller, R.K. Bergmann, M. Bachmann, J. Mihály, A. Gaál, B. Jezsó, B. Barátki, D. Kövesdi, S. Bősze, I. Szabó, T. Felföldi, E. Oszwald, P. Padmanabhan, B.Z. Gulyás, N. Hamdani, D. Máthé, Z. Varga, and K. Szigeti, Molecular imaging of bacterial outer membrane vesicles based on bacterial surface display. SCIENTIFIC REPORTS, 2023. 13(1).
2. Szöllősi, D., N. Hegedűs, D. Veres, I. Futo, I. Horvath, N. Stelczerné Kovács, B. Martinecz, Á. Dénes, D. Seifert, R. Bergmann, O. Lebeda, Z. Varga, Z. Kaleta, K. Szigeti, and D. Máthé, Evaluation of Brain Nuclear Medicine Imaging Tracers in a Murine Model of Sepsis-Associated Encephalopathy. MOLECULAR IMAGING AND BIOLOGY, 2018. 20(6): p. 952-962.

Publications not related to the thesis

1. Arndt, C., R.K. Bergmann, F. Striese, K.G. Merkel, D. Máthé, L.R. Loureiro, N. Mitwasi, A. Kegler, F. Fasslrinner, S.K.E. González, C. Neuber, N. Berndt, N. Kovács, D. Szöllősi, N. Hegedűs, G. Tóth, J.P. Emmermann, K.B. Harikumar, T. Kovács, M. Bachmann, and A. Feldmann, Development and Functional Characterization of a Versatile Radio-/Immunotheranostic Tool for Prostate Cancer Management. CANCERS, 2022. 14(8).
2. Bastian, M.B., A.M. Konig, S. Viniol, M. Gyánó, D. Szöllősi, I. Góg, J. Kiss, S. Osváth, K. Szigeti, A.H. Mahnken, and R.P. Thomas, Digital Variance Angiography in Lower-Limb Angiographywith Metal Implants. CARDIOVASCULAR AND INTERVENTIONAL RADIOLOGY, 2021. 44(3): p. 452-459.
3. Császár, E., N. Lénárt, C. Cserép, Z. Környei, R. Fekete, B. Pósfai, D. Balázsfi, B. Hangya, D.A. Schwarcz, E. Cserépné Szabadits, D. Szöllősi, K. Szigeti, D. Máthé, B.L. West, K. Tóthné Sviatkó, A.R. Brás, J.-C. Mariani, A. Kliewer, Z. Lenkei, L. Hricisák, Z. Benyó, M. Baranyi, B. Sperlágh, Á. Menyhárt, E. Farkas, and Á. Dénes, Microglia modulate blood flow, neurovascular coupling, and hypoperfusion via purinergic actions. JOURNAL OF EXPERIMENTAL MEDICINE, 2022. 219(3).

4. David, T., V. Hlinova, V. Kubicek, R. Bergmann, F. Striese, N. Berndt, D. Szöllősi, T. Kovács, D. Máthé, M. Bachmann, H.-J. Pietzsch, and P. Hermann, Improved Conjugation, 64-Cu Radiolabeling, in Vivo Stability, and Imaging Using Nonprotected Bifunctional Macrocyclic Ligands: Bis(Phosphinate) Cyclam (BPC) Chelators. JOURNAL OF MEDICINAL CHEMISTRY, 2018. 61(19): p. 8774-8796.
5. Gaál, A., T. Garay, I. Horváth, D. Máthé, D. Szöllősi, D. Veres, M.J. Thomas, T. Kovács, J. Tóvári, R.K. Bergmann, C. Streli, G. Szakács, J. Mihály, Z. Varga, and N. Szoboszlai, Development and In Vivo Application of a Water-Soluble Anticancer Copper Ionophore System Using a Temperature-Sensitive Liposome Formulation. PHARMACEUTICS, 2020. 12(5).
6. Gyánó, M., M. Berczeli, C. Csobay-Novák, D. Szöllősi, I.V. Óriás, I. Góg, J. Kiss, D. Veres, K. Szigeti, S. Osváth, Á.A. Pataki, V. Juhász, Z. Oláh, P. Sótonyi, and B. Nemes, Digital variance angiography allows about 70% decrease of DSA-related radiation exposure in lower limb X-ray angiography. SCIENTIFIC REPORTS, 2021. 11(1).
7. Juriga, D., E.É. Kálmán, K. Juriga-Tóth, D. Barczikai, D. Szöllősi, A. Földes, G. Varga, M. Zrínyi, A. Jedlovszky-Hajdú, and K. S. Nagy, Analysis of Three-Dimensional Cell Migration in Dopamine-Modified Poly(aspartic acid)-Based Hydrogels. GELS (BASEL), 2022. 8(2).
8. Kálmán, M., L. Tóth, D. Szöllősi, E. Oszwald, J. Mahalek, and S. Sadeghian, Correlation between extravasation and alterations of cerebrovascular laminin and β-dystroglycan immunoreactivity following cryogenic lesions in rats. JOURNAL OF NEUROPATHOLOGY AND EXPERIMENTAL NEUROLOGY, 2017. 76(11): p. 929-941.
9. Keszthelyi, S., D. Szöllősi, L. Strobel, S. Osváth, K. Szigeti, Z. Pónya, Á. Csóka, and T. Donkó, Novel, X-ray supported kinetic imaging of hidden-lifestyle arthropods. INSECT SCIENCE, 2021. 28(1): p. 281-284.
10. Merkel, K.G., D. Szöllősi, I. Horváth, B. Jezsó, Z. Baranyai, K. Szigeti, Z. Varga, I. Hegedüs, P. Padmanabhan, B. Gulyás, R.K. Bergmann, and D. Máthé, Radiolabeling of Platelets with 99mTc-HYNIC-Duramycin for In Vivo Imaging Studies. INTERNATIONAL JOURNAL OF MOLECULAR SCIENCES, 2023. 24(23).
11. Óriás, I.V., M. Gyánó, I. Góg, D. Szöllősi, D. Veres, Z. Nagy, C. Csobay-Novák, Z. Oláh, J. Kiss, S. Osváth, K. Szigeti, Z. Ruzsa, and P. Sótonyi, Digital Variance Angiography as a Paradigm Shift in

Carbon Dioxide Angiography. INVESTIGATIVE RADIOLOGY, 2019. 54(7): p. 428-436.
12. Óriás, I.V., D. Szöllősi, M. Gyánó, D. Veres, S. Nardai, C. Csobay-Novák, B. Nemes, J. Kiss, K. Szigeti, S. Osváth, P. Sótonyi, and Z. Ruzsa, Initial evidence of a 50% reduction of contrast media using digital variance angiography in endovascular carotid interventions. European Journal of Radiology Open, 2020. 7.
13. Ritter, Z., K. Zámbó, P. Balogh, D. Szöllősi, X. Jia, Á. Balázs, G. Taba, D. Dezső, I. Horváth, H. Alizadeh, D. Tuch, K. Vyas, N. Hegedűs, T. Kovács, K. Szigeti, D. Máthé, and E. Schmidt, In situ lymphoma imaging in a spontaneous mouse model using the Cerenkov Luminescence of F-18 and Ga-67 isotopes. SCIENTIFIC REPORTS, 2021. 11(1).
14. Ritter, Z., K. Zámbó, X. Jia, D. Szöllősi, D. Dezső, H. Alizadeh, I. Horváth, N. Hegedűs, D. Tuch, K. Vyas, P. Balogh, D. Máthé, and E. Schmidt, Intraperitoneal glucose transport to micrometastasis: A multimodal in vivo imaging investigation in a mouse lymphoma model. INTERNATIONAL JOURNAL OF MOLECULAR SCIENCES, 2021. 22(9).
15. Szigeti, K., N. Hegedűs, K. Rácz, I. Horváth, D. Veres, D. Szöllősi, I. Futó, K. Módos, T. Bozó, K. Karlinger, N. Stelczerné Kovács, Z. Varga, M. Babos, F.C. Budán, P. Padmanabhan, B. Gulyás, and D. Máthé, Thallium Labeled Citrate-Coated Prussian Blue Nanoparticles as Potential Imaging Agent. CONTRAST MEDIA & MOLECULAR IMAGING, 2018. 2018.
16. Szöllősi, D., L. Toth, and M. Kálmán, Postmortem immunohistochemical alterations following cerebral lesions: A possible pathohistological importance of the beta-dystroglycan immunoreactivity. NEUROPATHOLOGY, 2018. 38(3): p. 207-217.
17. Thomas, R.P., M.B. Bastian, S. Viniol, A.M. König, S.S. Amin, O. Eldergash, J. Schnabel, M. Gyánó, D. Szöllősi, I. Góg, J. Kiss, S. Osváth, K. Szigeti, and A.H. Mahnken, Digital Variance Angiography in Selective Lower Limb Interventions. JOURNAL OF VASCULAR AND INTERVENTIONAL RADIOLOGY, 2022. 33(2): p. 104-112.
18. Tóth, L., D. Szöllősi, K. Kis-Petik, I. Adorján, F. Erdélyi, and M. Kálmán, The First Postlesion Minutes: An In Vivo Study of Extravasation and Perivascular Astrocytes Following Cerebral Lesions in Various Experimental Mouse Models. JOURNAL OF HISTOCHEMISTRY & CYTOCHEMISTRY, 2019. 67(1): p. 29-39.

19. Tóth, L., D. Szöllősi, K. Kis-Petik, E. Oszwald, and M. Kálmán, Early phenomena following cryogenic lesions of rat brain - a preliminary study. ACTA BIOLOGICA SZEGEDIENSIS, 2015. 59: p. 361-369.

∑IF: 87.893